photonics

MDPI

Article

Wavelength-Tunable Chirped Pulse Amplification System (1720 nm–1800 nm) Based on Thulium-Doped Fiber

Xinyang Liu [1,*] and Regina Gumenyuk [1,2]

[1] Laboratory of Photonics, Tampere University, Korkeakoulunkatu 3, 33720 Tampere, Finland; regina.gumenyuk@tuni.fi
[2] Tampere Institute for Advanced Study, Tampere University, Kalevantie 4, 33100 Tampere, Finland
* Correspondence: xinyang.liu@tuni.fi

Abstract: Chirped pulse amplification (CPA) has been a commonly used methodology to obtain powerful ultrashort laser pulses ever since its first demonstration. However, wavelength-tunable CPA systems are much less common. Wavelength-tunable ultrashort and intense laser pulses are desirable in various fields such as nonlinear spectroscopy and optical parametric amplification. In this work, we report a 1720 nm–1800 nm tunable CPA system based on Tm-doped fiber. The tunable CPA system contains a seed laser, a pulse stretcher, two cascaded amplifiers and a pulse compressor. The dispersion-managed seed laser cavity emits wavelength-tunable laser pulses with pulse durations of several ps and spectral widths from 25 nm to 34 nm. After being stretched temporally to tens of ps, the laser pulses are then amplified in two-stage amplifiers and compressed in a Treacy-type compressor. At 1720 nm, the maximum average power of 126 mW is obtained with a pulse duration of 507 fs; at 1800 nm, the maximum average power of 264 mW is obtained with a pulse duration of 294 fs. The pulse repetition rates are around 22.7 MHz. We perform an analysis of the system design based on numerical simulations and go on to suggest further steps for improvement. To the best of our knowledge, this is the first demonstration of a tunable CPA system beyond 1.1 μm. Considering the specific wavelength range, this wavelength-tunable CPA system is highly desirable for biomedical imaging, sensing, and parametric amplifiers.

Keywords: ultrashort pulses; tunable CPA system; Tm-doped fiber laser; third biological window

Citation: Liu, X.; Gumenyuk, R. Wavelength-Tunable Chirped Pulse Amplification System (1720 nm–1800 nm) Based on Thulium-Doped Fiber. *Photonics* **2024**, *11*, 439. https://doi.org/10.3390/photonics11050439

Received: 18 April 2024
Revised: 6 May 2024
Accepted: 7 May 2024
Published: 8 May 2024

1. Introduction

The concept of the CPA technique originated from the approach of radar development aimed at using a high-energy exploratory radio pulse and a short detecting radio pulse to achieve a long detection range whilst retaining good range resolution [1,2]. In 1985, after about four decades of development, this concept was applied to laser pulse amplification [3]. Thereafter, the laser peak power level was able to break through the gigawatt bottleneck and continue to grow [4]. Since then, CPA became the golden rule for achieving high-power ultrashort laser pulses. The CPA technique has enabled the generation of ultrahigh-intensity laser pulses and facilitated many light–matter interaction applications, such as laser fusion, electron acceleration, and harmonic generation [4].

Basically, the CPA technique enables the laser intensity to be increased by preventing the accumulation of detrimental nonlinear effects that occur when light propagates in nonlinear waveguides, including both the Kerr and Raman nonlinearities. In a typical CPA setup, the low-power laser pulse generated by the seed laser is stretched temporally before it is amplified, thus retaining low pulse peak power in the amplifier and avoiding the accumulation of too much nonlinearity. The amplification stage usually includes several amplifiers. After being amplified, the laser pulse is recompressed in a pulse compressor. In its early years, the CPA technique was mostly used in Ti: Sapphire and Nd-doped solid-state laser systems [5,6]. Gradually, this approach was applied more

widely in fiber laser systems, covering wavelengths ranging from 1 μm to 2 μm using Yb-, Er-, and Tm-doped active fibers [7–9]. There has been ample research into the CPA technique which has thoroughly covered the different stages of a CPA setup. The seed laser mainly determines the central wavelength of the system and its ultimate spectrum width. By engineering the laser cavities, wavelength-tunable and dual-wavelength lasers have been used in CPA systems to enable wavelength-tuning and dual-wavelength operation in Ti: Sapphire laser systems [10,11]. Broadband seed lasers have undergone dramatic development [12,13], although their amplification is restricted by the gain-narrowing effect. Some methods have been put forward to solve this problem, such as gain-managed nonlinear broadening [14,15]. For the stretcher, several kinds of wavelength-dispersive components have been employed, such as passive fiber, transmissive gratings, dispersive mirrors, and chirped bragger grating [3,11,16,17]. For the amplifier, different amplification media have been used to boost average power levels, including rare-earth-ion doped crystals, rare-earth-ion doped fibers, and rare-earth-ion doped photonic crystal fibers (PCF) [16–18]. The most commonly used type of compressor is a Treacy-type compressor consisting of two gratings since it is flexible and has a high damage threshold [19]. In addition, dispersive mirrors and PCF have also been exploited for pulse compression [16,20]. Self-phase modulation-induced pulse pedestals have been studied to improve the pulse quality in the CPA system, and various solutions have been put forward [6,21–23].

CPA has been studied for decades as an important technique for building powerful laser sources. However, most CPA systems can only work at one fixed wavelength. Wavelength tunability is a crucial feature of laser sources when it comes to laser applications such as microscopy, spectroscopy, and parametric amplifiers. In bio-imaging, one tunable laser source may cover several absorption peaks of various biological chromophores [24]. In parametric amplifiers, changing the wavelength of a tunable pump laser can alter the idler signal wavelength over a relatively large range [25]. In the past, tunable CPA systems have been achieved in Ti: Sapphire solid-state laser systems at around 800 nm and Yb-doped fiber laser systems at around 1 μm [11,26]. Gain bandwidth is one of the main limitations for the wavelength-tuning range. Compared with Er- and Yb-doped active materials, Tm-doped fiber can provide a wide emission wavelength band ranging from 1600 nm to 2200 nm [27]. This makes it a good active laser medium for a widely tunable CPA system. Notably, part of this wavelength range falls into the third biological window (1600 nm–1870 nm), which has already been proven to have a longer attenuation length than the first and second biological windows in some scattering tissues [24]. The relatively long wavelength can also aid a parametric amplifier in mid-infrared light generation to obtain high quantum efficiency. The 1.7 μm-band ultrafast operation of Tm-doped fiber laser has been extensively studied over the past few years, including both fixed wavelength and wavelength-tunable operation. The mode-locking techniques used have included nonlinear polarization rotation [28–31], a nonlinear amplifying loop mirror [32,33], material-based saturable absorbers [34,35], and synchronously pumped mode-locking [36]. The average output powers from the oscillators are at the mW level, resulting in pulse energies below 1 nJ. The pulse durations from the oscillator are typically several ps and can be compressed down to hundreds of fs externally. To improve the power level/pulse energy, the CPA technique has been applied after the seed laser. In 2017, Can Li et al. reported a CPA system based on a Tm-doped soliton fiber laser operating at 1785 nm that boosted the average power to 264 mW with a pulse energy of 5.7 nJ and a pulse duration of 445 fs [37]. In 2021, Shaoxiang Wang et al. demonstrated a CPA system based on W-type Tm-doped fiber at 1785 nm which delivered a pulse energy of 128 nJ whose duration was compressed to 174 fs using SMF28 fiber [32]. In the same year, Ji-Xiang Chen et al. demonstrated a CPA system based on commercial Tm-doped fiber at 1734 nm. This attained an average output power of 1.3 W with a pulse duration of 378 fs and a pulse energy of 54 nJ [38]. However, these CPA systems only worked at one fixed wavelength.

There are two main challenges to achieving tunable CPA operation. One is to provide a tunable seed laser for the amplifier, and the other is to suppress any detrimental ASE in the

amplifiers. Different strategies have been used to solve these challenges in the two tunable CPA systems described above [11,26]. In the tunable Ti: Sapphire CPA system [11], the seed laser, which is a commercial self-mode-locked Ti: Saphire laser, can provide wavelength-tunable laser pulses. Three mirror sets with different spectral coating ranges were used to suppress the ASE from the regenerative amplifier. In the tunable Yb-doped CPA fiber system [26], the tunable seed laser for the amplifier is provided by selecting part of the broadband emission spectrum from the oscillator using a free space tunable filter consisting of a grating pair, a slit, and two cylindrical lenses.

In this work, we present a widely tunable Tm-doped fiber-based CPA system operating from 1720 nm to 1800 nm. The wavelength-tunable seed laser works in a dissipative soliton regime using a dispersion-managed cavity. This delivers ps laser pulses with spectrum widths ranging from 25 nm to 34 nm. A length of normal-dispersion fiber is used to temporally stretch the laser pulses. After going through two-stage amplifiers based on single-mode Tm-doped fibers and one external compression stage, a maximum average output power of 126 mW is obtained at 1720 nm with 507 fs pulse duration and 5.5 nJ pulse energy. 264 mW average output power is obtained at 1800 nm with a pulse duration of 294 fs and pulse energy of 11.6 nJ. To suppress the amplified spontaneous emission (ASE) from the amplifiers at longer wavelengths, wavelength-dependent fiber bending loss is introduced before the amplifiers as a tunable filter. We also perform numerical simulations of the CPA system and suggest further improvements to the system's design. In addition to the two existing demonstrations of a tunable CPA system, we provide another solution for a tunable CPA system with an all-fiber configuration from the stretcher to the amplifiers. To our knowledge, this is the first report of a tunable CPA system in this wavelength region. This tunable CPA system was originally built for the European Union Horizon 2020 project—Advanced Multimodal Photonics Laser Imaging Tool for Urothelial Diagnosis in Endoscopy (AMPLITUDE) [39], and it can work as a versatile laser source for different applications.

2. Experiment, Results, and Discussion

The setup of the tunable CPA system based on single-mode fiber is shown in Figure 1. The cascaded multi-stage laser architecture is framed separately. This includes a seed laser, stretcher, first amplifier, second amplifier, and compressor. The seed laser has a dispersion-managed cavity composed of 9.37 m single-mode fiber and 41 cm free space. 80 cm Thulium-doped fiber (TDF, TmDF200, OFS) provides optical gain for the whole wavelength-tuning range (1720 nm–1800 nm). This is pumped by a 1550 nm laser via a wavelength-division multiplexer (WDM). A 5.7 m dispersion-compensating fiber (DCF1, UHNA4, Nufern, East Granby, CT, USA) is employed to shift the cavity net dispersion to being the slightly normal. The other fiber in the cavity is SMF28. The net dispersion of the cavity is around 0.0044 ps^2. Two quarter waveplates, one half waveplate, and an acousto-optic tunable filter (AOTF, AOTF8, AA Opto-Electronic, Orsay, France) are accommodated in the free space part and are responsible for nonlinear polarization rotation (NPR), mode-locking, and wavelength tuning. The polarization-independent isolator (ISO) is used to maintain unidirectional laser operation. One fused fiber coupler with a splitting ratio of 30/70 is used to couple out 70% optical power. After the seed laser, the next stage configured for pulse stretching is a 10 m DCF2 (DM1010-D, YOFC, Wuhan, China). The DCF2's normal dispersion is specified as 0.1275 ps^2/m–0.2167 ps^2/m at 1550 nm because it was originally designed for dispersion compensation at this wavelength. However, in our setup, apart from dispersion compensation, we take advantage of the highly wavelength-dependent bending loss of this fiber to suppress undesired amplified spontaneous emission (ASE) at a longer wavelength generated by TDF. For the first amplification stage, 70 cm TDF is used to provide gain. The length was determined by using a cutting-back method to achieve optimum amplification performance. After the 70 cm TDF, a 1.55 µm/1.75 µm WDM and a polarization-independent ISO are spliced sequentially to extract the residual pump and to prevent back reflection, respectively. After the ISO, 40 cm DCF2 is spliced

to filter out the ASE generated from the Amplifier1 stage. Another piece of 70 cm TDF is used in Amplifier2 to further enhance the output power. After Amplifier2, one grating pair (T-711-1650, LightSmyth Technologies, Eugene, OR, USA) compensates for the up-chirp of the laser pulse. One roof mirror (HRS1015-M01, Thorlabs, Newton, NJ, USA) is used to retroreflect the laser beam from the pulse compressor and separate the output laser beam from the incident beam in the vertical axis. The pump for the TDFs in the seed laser, Amplifier1, and Amplifier2 are provided by three self-made master oscillator power amplifiers (MOPA) at 1.55 µm with maximum average powers of 3 W. The MOPA system contains one low power commercial 1.55 µm laser diode (QDFBLD-1550-50, QPhotonics) as seed laser and 5 m Er-Yb co-doped fiber (SM-EYDF-10P/125-XP, COHERENT, Saxonburg, PA, USA) as an amplifier pumped with 976 nm multimode laser diode (K976AAHRN-27.00W, BWT, Mondsee, Austria).

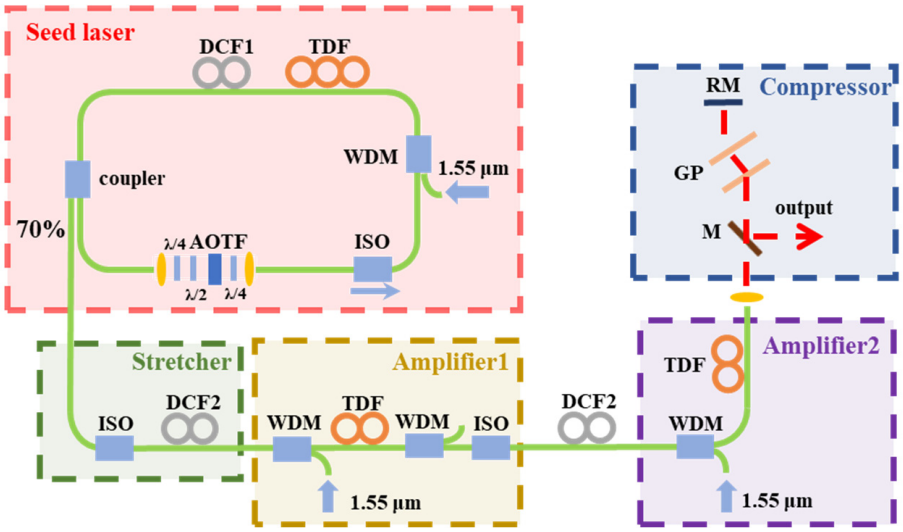

Figure 1. The setup of the tunable single-mode fiber based CPA system. WDM: wavelength-division multiplexer; TDF: Tm-doped fiber; DCF: dispersion-compensating fiber; λ/4: quarter waveplate; λ/2: half waveplate; AOTF: acousto-optic tunable filter; ISO: isolator; GP: grating pair; RM: roof mirror.

The seed laser is first operated in an all-anomalous-dispersion configuration. Once the soliton is in operation, DCF1 is added to shift the net cavity dispersion to being the slightly normal and to enable the laser to work in a dissipative soliton regime. The AOTF has a transmission bandwidth of around 12 nm in the operational wavelength region with a Gaussian-like transmission profile. Sweeping the frequency of the driving RF signal for the AOTF from 40 MHz to 38.2 MHz, the center wavelength of the AOTF can be changed from 1800 nm to 1720 nm. At 1720 nm, 1740 nm, 1760 nm, 1780 nm, and 1800 nm, the pump powers for the mode-locking operations are 1.06 W, 0.683 W, 0.584 W, 0.723 W, and 0.683 W, respectively. All the output spectra have a rectangular shape with spectral widths ranging from 25 nm to 34 nm, as shown in Figure 2a. The spectrum side lobes appearing on the long-wavelength side of the spectrum may come from the intrinsic property of acoustic diffraction [40]. The relatively flat spectrum top is a combined action of nonlinearity like self-phase modulation and normal dispersion in DCF1 [31], while the spectrum profile can also be affected by the intracavity spectral filtering effect and gain profile of TDF. The pulse durations after the seed laser vary from 5.8 ps to 8.1 ps, and the average output powers are from 5.45 mW to 9.3 mW, as illustrated in Figure 2b. A typical pulse train is shown in Figure 2c. The variation in the output parameters at different wavelengths is caused by changes in the intracavity parameters (dispersion, nonlinearity, gain, and loss) within the tuning wavelength range. Consequently, there is a need to adjust the performance of the NPR to maintain stable mode-locking operation. The adjustment of NPR performance,

i.e., rotation of waveplates, affects the Lyot spectral filter formed inside the cavity and the saturation intensity and modulation depth of the artificial saturable absorber.

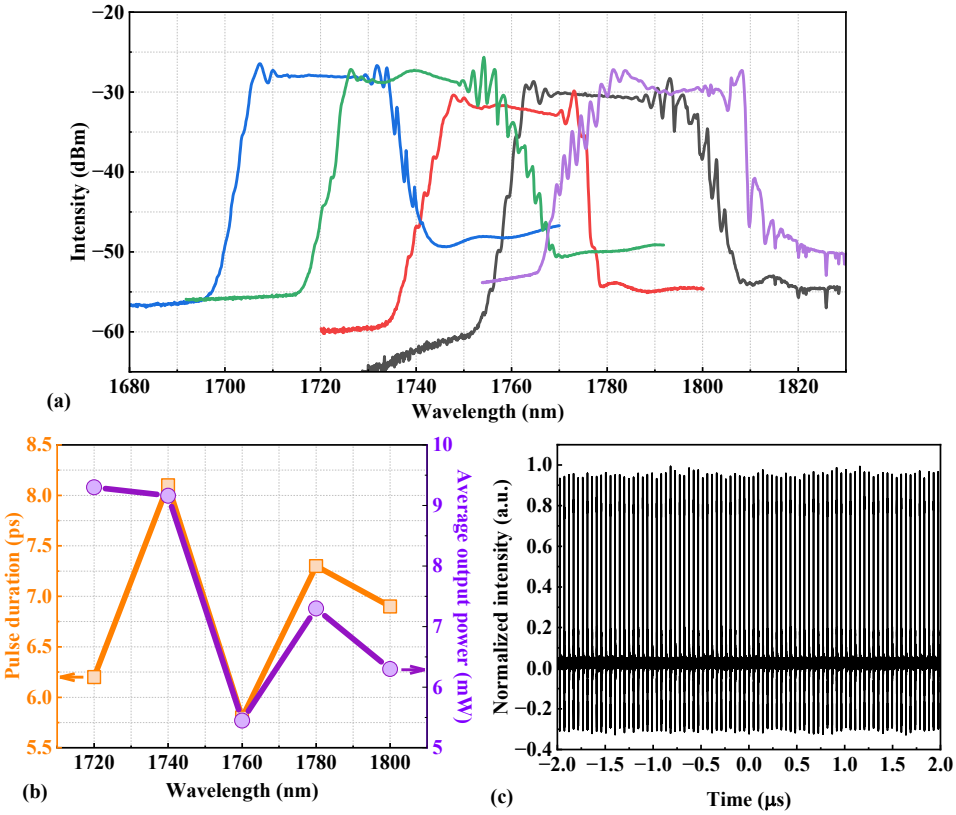

Figure 2. The tunable seed laser performance: (**a**) the optical spectra with different colored lines showing spectrum at different wavelength, (**b**) the pulse durations and average output powers, and (**c**) a typical pulse train.

The laser pulses from the seed laser are subsequently stretched in the 10 m DCF2 up to ~50 ps at 1740 nm measured with a fast photodetector with 25 GHz bandwidth (Newport 1414) and an oscilloscope with a 20 GHz bandwidth and a 50 GS/s sampling rate (Tektronix DSA 72004). Since we are aiming for several hundred mW average output power, the pulse duration is considered suitable for the following amplification. The amplification is first performed at the shortest wavelength of 1720 nm. As this wavelength is at the short edge of the Tm-doped fiber gain profile, we note the rise of ASE in the long-wavelength region from each stage of the CPA system, consisting of the TDF (seed laser, Amplifier1, and Amplifier2). Therefore, it is necessary to introduce long-wavelength ASE suppression. The DCF2 fiber features highly wavelength-dependent bending-induced losses due to its small core area. This results in the discrimination of the waveguiding conditions for different wavelengths. The DCF2 fiber after Amplifier1 is carefully bent by forming fiber rings with a diameter of ~10 cm to suppress the ASE beyond 1742 nm [31]. In practical implementation, the DCF2 fiber is first coiled to introduce an approximate loss, then fine bending of DCF2 fiber should be tailored carefully to suppress unwanted ASE while preserving the laser signal. At maximum pump power (3 W) for both Amplifier1 and Amplifier2, we characterize the output from Amplifier2. Figure 3a illustrates the effect of introducing the bending loss of DCF2 to suppress the ASE at longer wavelengths. With the bending loss, the ASE can be suppressed by 13 dB and the ASE spectral peak shifts from 1771 to 1758 nm, indicating the wavelength-dependent bending loss mechanism can be effectively used as an ASE filter. It is notable that the same DCF is also used for introducing the temporal stretching. This simplifies the scheme's design and decreases the number of needed components. The suppression of the long-wavelength ASE improves the signal

spectrum extinction ratio (peak to ASE peak ratio) from 9.7 dB to more than 19 dB. Due to the gain-narrowing effect, the 5-dB spectrum width is severely decreased from 29 nm (after the seed laser) to 10 nm (after Amplifier2). The maximum output power after Amplifier2 is 210 mW, resulting in a pulse energy of 9.3 nJ. To compress the pulse, the pulse duration after Amplifier2 is measured to be ~51 ps. Together with the spectrum width, the grating pair distance is determined to be around 20 cm. Note that the theoretically accumulated chirp is calculated by assuming that the laser pulse has a perfect Gaussian shape, which is hardly ever the actual pulse shape in practice. Thus, the grating pair distance should be adjusted accordingly by measuring the pulse duration variation with the grating pair distance. By setting the grating pair distance at 19.7 cm, the pulse duration can be compressed to the shortest duration of 507 fs (Figure 3b), assuming a hyperbolic secant ($sech^2$) pulse shape. 126 mW average power is left due to the loss introduced by the grating pair.

The next step is to perform the amplification at 1800 nm. First, the wavelength of the seed laser is tuned to 1800 nm by changing the frequency of the driving RF signal for the AOTF. The dissipative soliton operation can be obtained by setting the waveplates at suitable angles. For the following amplification, the DCF2 bending is released as this wavelength is close to the gain peak and the ASE at other wavelengths is not pronounced. In contrast to case at 1720 nm, the gain-narrowing effect is dramatically alleviated due to the relatively flat gain at 1800 nm. The spectral width after Amplifier2 is almost the same as the one after the seed laser, both of which are ~27 nm. The signal-to-ASE ratio of the spectrum is about 20 dB. No nonlinearity caused by spectrum distortion is observed. The maximum output power after Amplifier2 is 409 mW. By setting the grating pair distance at 10.3 cm, the pulse duration can be compressed to 294 fs (Figure 3d) with an average output power of 264 mW and a pulse energy of 12.7 nJ. The pedestal in Figure 3d indicates that there is some nonlinear chirp left in the compressed pulse. However, the total power concentrated in the pedestal is only about 15%. Since we employ the NPR technique for mode-locking in a laser cavity constructed by non-polarization maintaining fibers, the polarization state of seed laser output is expected to be elliptically polarized. The following stages of stretcher, amplifiers, and pulse compressor do not contain polarizing components. Thus the output after compressor is also expected to be elliptically polarized.

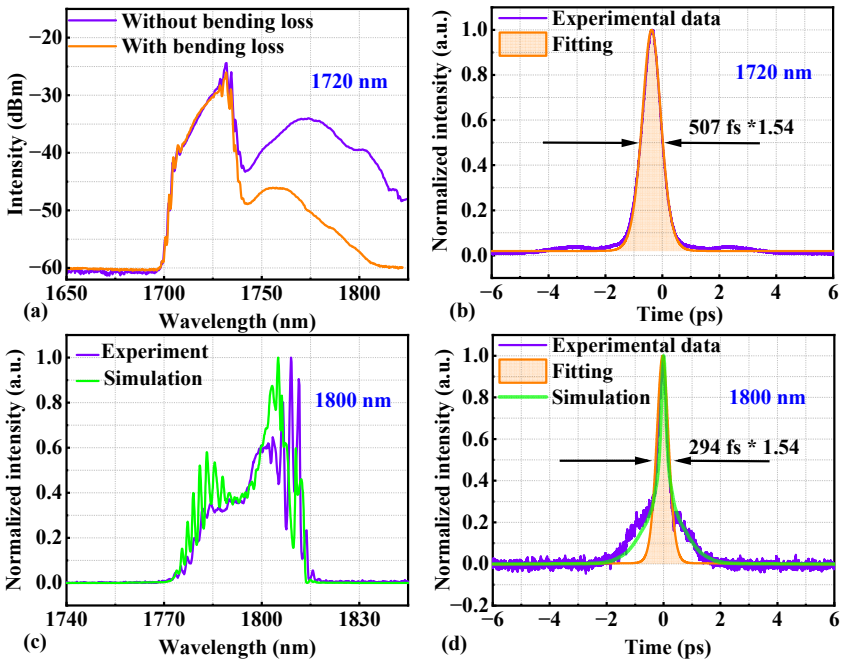

Figure 3. Spectra after the Amplifier2 (**a**,**c**) and autocorrelation traces of compressed pulse (**b**,**d**) at two wavelengths 1720 and 1800 nm. The green lines in (**c**,**d**) are the simulated results of the CPA system at 1800 nm.

3. Simulation

The experimental outputs of the CPA system at 1800 nm are numerically validated by solving the generalized nonlinear Schrödinger equation (GNLSE) using the split-step Fourier method based on the second-order Runge–Kutta Algorithm [41,42]:

$$\frac{\partial A}{\partial z} + i\frac{\beta_2}{2}\frac{\partial^2 A}{\partial T^2} + \frac{\beta_3}{6}\frac{\partial^3 A}{\partial T^3} = \frac{g}{2} + i\gamma\left(1 + i\tau_{stock}\frac{\partial}{\partial T}\right)\left(A\int_{-\infty}^{\infty} R(t)|A(z, T-t)|^2 dt\right), \quad (1)$$

where $A(z, T)$ is the complex electrical field; z is the coordinate of the pulse propagation; T is the time coordinate moving at the group velocity of the pulse; β_2 is the group velocity dispersion (GVD); β_3 is the third-order dispersion (TOD) parameter; g represents the gain parameter for Tm-doped fiber; γ is the nonlinear coefficient and can be calculated by $2\pi n_2/(\lambda A)$, where n_2 is the nonlinear refractive index, λ is the wavelength, A is the mode area; τ_{stock} is the shock-formation time-scale that is responsible for the self-steeping effect; and $R(t)$ is the response function that models both the instantaneous electronic (Kerr) nonlinearity and the delayed molecular (Raman) nonlinearity [43]. The gain coefficient is simulated using the saturable model:

$$g = \frac{g_0}{1 + \frac{E_{pulse}}{E_{sat}}}, \quad (2)$$

where g_0 is the small-signal gain coefficient with values following the gain profile, E_{pulse} is the pulse energy, and E_{sat} is the gain saturation energy. In passive fiber, the gain coefficient is set at zero. E_{pulse} can be calculated by the following equation:

$$E_{pulse} = \int_0^{\tau_{win}} |A(z, t)|^2 dt, \quad (3)$$

where τ_{win} is the simulation window size. E_{sat} is set to be 2 pJ for Tm-doped fibers.

The simulation starts from the experimentally obtained spectrum and pulse duration after the seed laser at 1800 nm. The phase information is lost in the power spectrum and autocorrelation measurements. We assume the laser pulse after the seed laser is up-chirped with the linear chirp/parabolic phase. By adding a parabolic phase profile with proper parameters to the spectrum field, an up-chirped pulse in the temporal domain with a 6.9 ps pulse duration can be obtained. This 6.9 ps pulse then goes through the 10 m DCF2, 30 cm SMF28, 70 cm TDF, 60 cm SMF28, 40 cm DCF2, 30 cm SMF28, 70 cm TDF, and a pulse compressor (Figure 4). The three pieces of SMF28 are intended to simulate the fiber pigtails of the components. In the simulation, we approximate the following values to match the output temporal and spectral profiles with the experimental results: β_2 is set to be 0.21 ps^2/m, -0.058 ps^2/m, and -0.08 ps^2/m for the DCF2, SMF28, and TDF, respectively. β_3 is set to be 2.9536×10^{-3} ps^3/m for all fibers, and n_2 is set to be 3×10^{-20} m^2/W for all fibers. The small-signal gain coefficient g_0 is set to be 2500 m^{-1} and 6300 m^{-1} for the TDFs in Amplifier1 and Amplifier2, respectively. The values for g_0 are chosen to obtain similar pulse energies in the simulation as in the experimental ones. The group delay dispersion (GDD) and the TOD of the pulse compressor are set to be -2.6 ps^2 and 1.66×10^{-2} ps^3, respectively. These values are very close to the experimental setting of the 711 lines/mm grating pair with a 10.3 cm distance and a 37° angle. The minor deviation between the simulated spectrum and autocorrelation trace and the experimental ones (Figure 3c,d) confirms their conformance. Once we find the corresponding simulation parameters needed to match the output pulse shape with the experimental results, we vary them in order to investigate the CPA system's limiting conditions and to formulate further improvements.

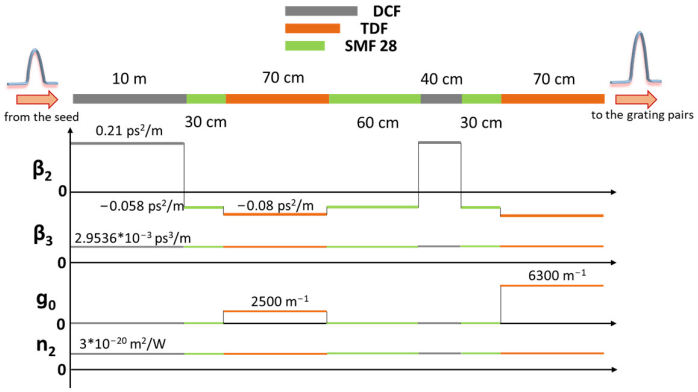

Figure 4. A map of the parameters used for the CPA system simulations at 1800 nm.

We note that in our previous study [31] we demonstrated the wavelength-tunable dissipative soliton operation of a Tm-doped fiber laser from 1.7 µm to 1.9 µm and validated its wide-band capability to be amplified by a stretcher-free one-stage amplifier. In this work, we first optimized the seed laser cavity dispersion and cavity loss. Compared with Ref. [31], the spectrum widths of the seed laser are increased by a factor of 1.2 to 3.1 for the different wavelengths, and the output powers are increased by a factor of 1.3 to 3.9. We also introduced the stretcher stage to build a classic CPA laser system and increased the length of the active fibers in the amplifier stages to boost the output performance.

Table 1 summarizes the amplification performances at the two wavelengths of Ref. [31] and this work. While both studies achieved compressed pulse durations of around 500 fs at the shortest wavelengths, this study achieved half the time-bandwidth product (TBP) of the study in Ref. [31]. The total length of the TDF in the two-stage amplifier in this study is about twice that of the one in Ref. [31]. The longer fiber length enhances the gain at longer wavelengths and results in a stronger narrowing effect at shorter wavelengths, thus limiting the obtainable shortest pulse duration near the 1700 nm edge. However, the addition of a stretcher improved the compressibility after the amplifier due to a decrease in the accumulated nonlinearity. Furthermore, the pulse energy in this study was nearly five times higher than that of Ref. [31]. In this latest study, at around 1800 nm, the compressed pulse duration was 294 fs. This is in stark contrast to the 478 fs achieved in Ref. [31]. The shorter pulse duration results from the slightly broader spectrum (27 nm in this work, 23 nm in Ref. [31]), as well as the improved pulse compressibility due to the addition of a stretcher. The pulse energy after the compressor is roughly double in this work, at 1800 nm. The TBPs at the two wavelengths implies that there are still some residual chirps in the compressed pulse. These could be caused by the positive third-order dispersion from the fibers and the accumulated nonlinearity. Although the addition of a stretcher can improve pulse compressibility, the total accumulated third-order dispersion in the chain of amplifiers and the stretcher is also increased. This suggests that there is a trade-off between high output power and short pulse duration, which should be considered when designing a CPA system. The wavelength region in this work is novel, and the component base is not well-developed. The choice of a single-mode fiber with normal dispersion for the stretcher was determined by the relatively large mode field diameter which resulted in minimization of the accumulated nonlinearity. However, this fiber is featured in the TOD of the same sign as for SMF 28 leading to its summing up and negative impact on the pulse compressibility. The use of a specially engineered fiber as UNH7 [44] with negative third-order dispersion in this wavelength region would compensate for the impact of this parameter on the pulse compressibility. However, this fiber has a 1.5 times smaller mode field diameter, which inevitably leads to an increase in nonlinearity and splicing losses. Therefore, any further improvements in the tunable CPA system for the wavelength region 1700–1800 nm would require the development of new components, such as fiber Bragg grating or large normal dispersion fiber with negative third-order dispersion. This would minimize the length

of the stretcher and the negative impact of the accumulated nonlinearity. Also, the wide tunability of the CPA system needs to match the dispersion parameter, which varies with wavelength, and this is a very challenging task. It is noteworthy that the available pump powers limit the maximum output powers with this CPA system. By using a stronger pump and engineering the CPA structure accordingly (such as introducing a stronger pulse-stretching effect and using large mode-area gain fiber, etc.), higher output power could be obtained. Nevertheless, we demonstrate here a novel, technically feasible route to realizing a tunable CPA system, and this is the first wavelength-tunable CPA system in this wavelength band.

Table 1. Comparison of output performances between Ref. [31] and this work.

Parameters	Ref. [31]		This Work	
Wavelength (nm)	1708	1807	1720	1800
Compressed pulse duration (fs)	523	478	507	294
Pulse energy after compressor (nJ)	1.19	4.3	6	12.7
TBP	1.01	0.914	0.514	0.735

4. Conclusions

We have demonstrated a wavelength-tunable CPA system operating from 1720 nm to 1800 nm composed of only single-mode fibers. The Tm-doped fiber seed laser operates in a dissipative soliton regime, and the intracavity tunability of the central wavelength is enabled by ATOF. The generated pulses are temporally stretched and sequentially amplified in a two-stage cascaded amplification system. When amplifying the laser pulse signal at 1720 nm, the strong ASE at longer wavelengths was effectively suppressed by 13 dB at the ASE peak. This was achieved by introducing wavelength-dependent bending loss in the DCF2. At the shortest wavelength of 1720 nm, the tunable CPA system delivered 507 fs compressed pulse duration with 126 mW output power. At the longest wavelength of 1800 nm, the maximum output power was 264 mW with 294 fs compressed pulse duration. In-depth analysis of the system design with the support of numerical simulations revealed further steps for future improvements to the system. Wavelength tunability of high-power ultrafast lasers is highly desirable in laser applications based on sensing or imaging techniques. Having the merits of flexibility and compactness, this tunable CPA system is a strong contender for that role among similar laser sources.

Author Contributions: Conceptualization, X.L. and R.G.; Funding acquisition, R.G.; Investigation, X.L.; Methodology, X.L. and R.G.; Project administration, R.G.; Supervision, R.G.; Visualization, X.L. and R.G.; Writing—original draft, X.L.; Writing—review and editing, X.L. and R.G. All authors have read and agreed to the published version of the manuscript.

Funding: This research was funded by the European Union's Horizon 2020 research and innovation program, grant number 871277, and by the Research Council of Finland, grant number 320165.

Data Availability Statement: Data underlying the results presented in this paper are not publicly available at this time but may be obtained from the authors upon reasonable request.

Conflicts of Interest: The authors declare no conflicts of interest.

References

1. Dicke, R.H. Object Detection Systems. U.S. Patent US616382A, 6 January 1953.
2. Darlington, S. Pulse Transmission. U.S. Patent US2678997A, 18 May 1954.
3. Strickland, D.; Mourou, G. Compression of Amplified Chirped Optical Pulses. *Opt. Commun.* **1985**, *56*, 219–221. [CrossRef]
4. Mourou, G.A.; Barry, C.P.J.; Perry, M.D. Ultrahigh-Intensity Lasers: Physics of the Extreme on a Tabletop. *Phys. Today* **1998**, *51*, 22–28. [CrossRef]
5. Maine, P.; Strickland, D.; Bado, P.; Pessot, M.; Mourou, G. Generation of Ultrahigh Peak Power Pulses by Chirped Pulse Amplification. *IEEE J. Quantum Electron.* **1988**, *24*, 398–403. [CrossRef]

6. Barty, C.P.J.; Guo, T.; Blanc, C.L.; Raksi, F.; Rose-Petruck, C.; Squier, J.; Wilson, K.R.; Yakovlev, V.V.; Yamakawa, K. Generation of 18-Fs, Multiterawatt Pulses by Regenerative Pulse Shaping and Chirped-Pulse Amplification. *Opt. Lett.* **1996**, *21*, 668–670. [CrossRef]
7. Yang, L.-M.; Stock, M.L.; Mourou, G.; Galvanauskas, A.; Fermann, M.E.; Harter, D.J. Chirped Pulse Amplification of Ultrashort Pulses Using Neodymium-and Erbium-Doped Fiber Amplifiers. In Proceedings of the TuD.23 International Conference on Ultrafast Phenomena (UP) 1994, Anaheim, CA, USA, 8–13 May 1994.
8. Imeshev, G.; Hartl, I.; Fermann, M.E. An Optimized Er Gain Band All-Fiber Chirped Pulse Amplification System. *Opt. Express* **2004**, *12*, 6508–6514. [CrossRef]
9. Haxsen, F.; Wandt, D.; Morgner, U.; Neumann, J.; Kracht, D. Pulse Energy of 151 nJ from Ultrafast Thulium-Doped Chirped-Pulse Fiber Amplifier. *Opt. Lett.* **2010**, *35*, 2991–2993. [CrossRef]
10. Zhang, Z.; Deslauriers, A.M.; Strickland, D. Dual-Wavelength Chirped-Pulse Amplification System. *Opt. Lett.* **2000**, *25*, 581–583. [CrossRef]
11. Yamakawa, K.; Magana, A.; Chiu, P.H. Tunable Ti: Sapphire Regenerative Amplifier for Femtosecond Chirped-Pulse Amplification. *Appl. Phys. B* **1994**, *58*, 323–326. [CrossRef]
12. Chichkov, N.B.; Hapke, C.; Neumann, J.; Kracht, D.; Wandt, D.; Morgner, U. Pulse Duration and Energy Scaling of Femtosecond All-Normal Dispersion Fiber Oscillators. *Opt. Express* **2012**, *20*, 3844–3852. [CrossRef]
13. Ma, C.; Khanolkar, A.; Zang, Y.; Chong, A. Ultrabroadband, Few-Cycle Pulses Directly from a Mamyshev Fiber Oscillator. *Photonics Res.* **2020**, *8*, 65–69. [CrossRef]
14. Sidorenko, P.; Fu, W.; Wise, F. Nonlinear Ultrafast Fiber Amplifiers beyond the Gain-Narrowing Limit. *Optica* **2019**, *6*, 1328–1333. [CrossRef] [PubMed]
15. Tomaszewska-Rolla, D.; Lindberg, R.; Pasiskevicius, V.; Laurell, F.; Soboń, G. A Comparative Study of an Yb-Doped Fiber Gain-Managed Nonlinear Amplifier Seeded by Femtosecond Fiber Lasers. *Sci. Rep.* **2022**, *12*, 404. [CrossRef] [PubMed]
16. Pervak, V.; Ahmad, I.; Trushin, S.A.; Major, Z.; Apolonski, A.; Karsch, S.; Krausz, F. Chirped-Pulse Amplification of Laser Pulses with Dispersive Mirrors. *Opt. Express* **2009**, *17*, 19204–19212. [CrossRef] [PubMed]
17. Sims, R.A.; Kadwani, P.; Ebendorff-Heideprem, H.; Shah, L.; Monro, T.M.; Richardson, M. Chirped Pulse Amplification in Single Mode Tm:Fiber Using a Chirped Bragg Grating. *Appl. Phys. B* **2013**, *111*, 299–304. [CrossRef]
18. Zhao, Z.; Kobayashi, Y. Ytterbium Fiber-Based, 270 Fs, 100 W Chirped Pulse Amplification Laser System with 1 MHz Repetition Rate. *Appl. Phys. Express* **2015**, *9*, 012701. [CrossRef]
19. Treacy, E. Optical Pulse Compression with Diffraction Gratings. *IEEE J. Quantum Electron.* **1969**, *5*, 454–458. [CrossRef]
20. Wei, R.; Wang, M.; Zhu, Z.; Lai, W.; Yan, P.; Ruan, S.; Wang, J.; Sun, Z.; Hasan, T. High-Power Femtosecond Pulse Generation From an All-Fiber Er-Doped Chirped Pulse Amplification System. *IEEE Photonics J.* **2020**, *12*, 1–8. [CrossRef]
21. Chuang, Y.-H.; Meyerhofer, D.D.; Augst, S.; Chen, H.; Peatross, J.; Uchida, S. Suppression of the Pedestal in a Chirped-Pulse-Amplification Laser. *J. Opt. Soc. Am. B* **1991**, *8*, 1226–1235. [CrossRef]
22. Perry, M.D.; Ditmire, T.; Stuart, B.C. Self-Phase Modulation in Chirped-Pulse Amplification. *Opt. Lett.* **1994**, *19*, 2149–2151. [CrossRef]
23. Braun, A.; Kane, S.; Norris, T. Compensation of Self-Phase Modulation in Chirped-Pulse Amplification Laser Systems. *Opt. Lett.* **1997**, *22*, 615–617. [CrossRef]
24. Sordillo, D.C.; Sordillo, L.A.; Sordillo, P.P.; Shi, L.; Alfano, R.R. Short Wavelength Infrared Optical Windows for Evaluation of Benign and Malignant Tissues. *J. Biomed. Opt.* **2017**, *22*, 045002. [CrossRef]
25. Andriukaitis, G.; Balčiūnas, T.; Ališauskas, S.; Pugžlys, A.; Baltuška, A.; Popmintchev, T.; Chen, M.-C.; Murnane, M.M.; Kapteyn, H.C. 90 GW Peak Power Few-Cycle Mid-Infrared Pulses from an Optical Parametric Amplifier. *Opt. Lett.* **2011**, *36*, 2755–2757. [CrossRef]
26. Shumakova, V.; Pecile, V.F.; Fellinger, J.; Leskowschek, M.; Aldia, P.E.C.; Mayer, A.S.; Perner, L.W.; Salman, S.; Fan, M.; Balla, P.; et al. Spectrally Tunable High-Power Yb:Fiber Chirped-Pulse Amplifier. *Photonics Res.* **2022**, *10*, 2309–2316. [CrossRef]
27. Jackson, S.D. Towards High-Power Mid-Infrared Emission from a Fibre Laser. *Nat. Photonics* **2012**, *6*, 423–431. [CrossRef]
28. Noronen, T.; Okhotnikov, O.; Gumenyuk, R. Electronically Tunable Thulium-Holmium Mode-Locked Fiber Laser for the 1700-1800 Nm Wavelength Band. *Opt. Express* **2016**, *24*, 14703. [CrossRef] [PubMed]
29. Emami, S.D.; Dashtabi, M.M.; Lee, H.J.; Arabanian, A.S.; Rashid, H.A.A. 1700 Nm and 1800 Nm Band Tunable Thulium Doped Mode-Locked Fiber Lasers. *Sci. Rep.* **2017**, *7*, 12747. [CrossRef]
30. Chen, J.-X.; Li, X.-Y.; Li, T.-J.; Zhan, Z.-Y.; Liu, M.; Li, C.; Luo, A.-P.; Zhou, P.; Wong, K.K.-Y.; Xu, W.-C.; et al. 1.7-Mm Dissipative Soliton Tm-Doped Fiber Laser. *Photonics Res.* **2021**, *9*, 873–878. [CrossRef]
31. Liu, X.; Sahu, J.K.; Gumenyuk, R. Tunable Dissipative Soliton Tm-Doped Fiber Laser Operating from 1700 Nm to 1900 Nm. *Opt. Lett.* **2023**, *48*, 612–615. [CrossRef]
32. Chen, S.; Chen, Y.; Liu, K.; Sidharthan, R.; Li, H.; Chang, C.J.; Wang, Q.J.; Tang, D.; Yoo, S. W-Type Normal Dispersion Thulium-Doped Fiber-Based High-Energy All-Fiber Femtosecond Laser at 1.7 Mm. *Opt. Lett.* **2021**, *46*, 3637. [CrossRef]
33. Lin, Z.-W.; Chen, J.-X.; Li, T.-J.; Zhan, Z.-Y.; Liu, M.; Li, C.; Luo, A.-P.; Zhou, P.; Xu, W.-C.; Luo, Z.-C. 1.7 Mm Figure-9 Tm-Doped Ultrafast Fiber Laser. *Opt. Express* **2022**, *30*, 32347. [CrossRef]
34. Dai, R.; Meng, Y.; Li, Y.; Qin, J.; Zhu, S.; Wang, F. Nanotube Mode-Locked, Wavelength and Pulsewidth Tunable Thulium Fiber Laser. *Opt. Express* **2019**, *27*, 3518–3527. [CrossRef] [PubMed]

35. Chen, S.; Chen, Y.; Liu, K.; Sidharthan, R.; Li, H.; Chang, C.J.; Wang, Q.J.; Tang, D.; Yoo, S. All-Fiber Short-Wavelength Tunable Mode-Locked Fiber Laser Using Normal Dispersion Thulium-Doped Fiber. *Opt. Express* **2020**, *28*, 17570–17580. [CrossRef] [PubMed]
36. Yang, H.; He, S. Widely Tunable 1.7 Mm Vector Dissipative Soliton All-Fiber Thulium Laser. *J. Light. Technol.* **2024**, *42*, 347–353. [CrossRef]
37. Li, C.; Wei, X.; Kong, C.; Tan, S.; Chen, N.; Kang, J.; Wong, K.K.Y. Fiber Chirped Pulse Amplification of a Short Wavelength Mode-Locked Thulium-Doped Fiber Laser. *APL Photonics* **2017**, *2*, 121302. [CrossRef]
38. Chen, J.-X.; Zhan, Z.-Y.; Li, C.; Liu, M.; Luo, A.-P.; Zhou, P.; Xu, W.-C.; Luo, Z.-C. 1.7 Mm Tm-Fiber Chirped Pulse Amplification System with Dissipative Soliton Seed Laser. *Opt. Lett.* **2021**, *46*, 5922–5925. [CrossRef] [PubMed]
39. Kurilchik, S.; Gacci, M.; Cicchi, R.; Pavone, F.S.; Morselli, S.; Serni, S.; Chou, M.H.; Närhi, M.; Rafailov, E.; Stewart, N.; et al. Advanced Multimodal Laser Imaging Tool for Urothelial Carcinoma Diagnosis (AMPLITUDE). *J. Phys. Photonics* **2020**, *2*, 021001. [CrossRef]
40. Dixon, R. Acoustic Diffraction of Light in Anisotropic Media. *IEEE J. Quantum Electron.* **1967**, *3*, 85–93. [CrossRef]
41. Dudley, J.M.; Genty, G.; Coen, S. Supercontinuum Generation in Photonic Crystal Fiber. *Rev. Mod. Phys.* **2006**, *78*, 1135–1184. [CrossRef]
42. Agrawal, G.P. Appendix D. In *Nonlinear Fiber Optics*, 6th ed.; Academic Press: Cambridge, MA, USA, 2019; pp. 693–694.
43. Runge, A.F.J.; Aguergaray, C.; Provo, R.; Erkintalo, M.; Broderick, N.G.R. All-Normal Dispersion Fiber Lasers Mode-Locked with a Nonlinear Amplifying Loop Mirror. *Opt. Fiber Technol.* **2014**, *20*, 657–665. [CrossRef]
44. Ciąćka, P.; Rampur, A.; Heidt, A.; Feurer, T.; Klimczak, M. Dispersion Measurement of Ultra-High Numerical Aperture Fibers Covering Thulium, Holmium, and Erbium Emission Wavelengths. *J. Opt. Soc. Am. B* **2018**, *35*, 1301. [CrossRef]